CHAPTER 2

EXPERIMENTAL

2.1 Materials

Chemical	Molecular formular	Molecular weight	Company
Titanium (IV) oxysulfate hydrate	$TiOSO_4$	159.92	Aldrich
Titanium dioxide, P25 Degussa	TiO_2	80.00	Degussa Germany
Ammonium hydroxide	NH_4OH	35.05	BDH England
Acetonitrile	CH_3CN	41.05	V.S.CHEM HOUSE
Benzoic acid	$C_7H_6O_2$	122.12	Merck Germany
Cinnamic acid	$C_9H_8O_2$	148.16	Merck Germany
Salicylic acid	$C_7H_6O_3$	138.12	Merck Germany
Oxalic acid	$C_2H_2O_4$	90.03	Aldrich
Percholric acid	$HClO_4$	100.47	Ajax

Chemical	Molecular formular	Molecular weight	Company
Sodium hydroxide	NaOH	40.00	Aldrich
Phenol	C_6H_6O	94.11	Aldrich

2.2 Instruments

1. UV-Vis diffuse reflectance spectroscope (UV-Vis DRS), Lambda650S
2. X-ray diffractometer (XRD), Rigaku MiniFlex II
3. Scanning electron microscopy, (SEM), JEOL JEM-6335F
4. Transmission electron microscope (TEM), JEOL JEM-2010
5. Brunauer-Emmett-Teller (BET), Micromeritics Tristar 3000
6. Fourier transform infrared spectrophotometer (FT-IR), 510 Nicolet
7. Zetasizer nano instrument , ZS Malvern
8. UVA-lamp, Sylvania blacklight blue, 18W
9. Spiral photoreactor
10. Conductivity meter, EUTECH PC 5500

2.3 Sample preparations

2.3.1 Preparation of TiO_2 catalysts

The thermal hydrolysis process was carried out using $TiOSO_4$ (>29% Ti (as TiO_2 basis), Aldrich), ammonia solution (28.0%, Aldrich) and deionized water. In a standard experiment, 10 g of $TiOSO_4$ was dissolved in 150 ml of deionized water at

room temperature. The solution was then heated to 80.0 ± 2.0 ºC for 1 h under constant stirring. After that ammonia solution was added dropwise until the solution pH was 7. The solution was left under stirring for a further 1 h. The schematic diagram for the preparation of TiO_2 is shown in Figure 2.1. The obtained white precipitate was washed several times with deionized water and then dried at 60 ºC for 24 h. The powder was calcined in air at 300-900 ºC for 3 h.

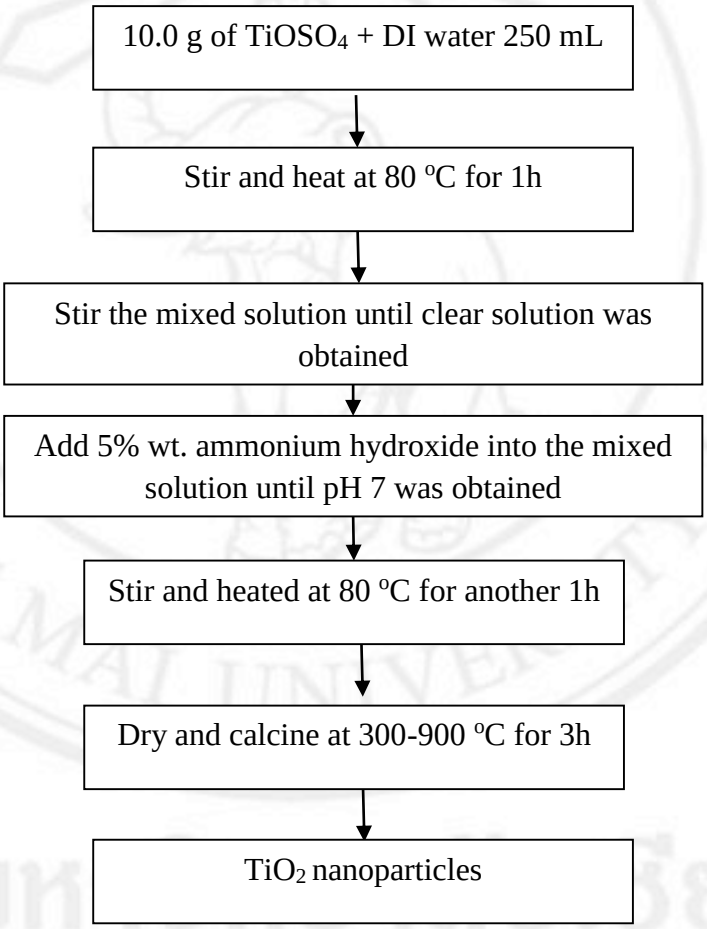

Figure 2.1 Schematic diagram of the preparation of TiO_2

2.3.2 TiO_2 modified with carboxylic acid

Modification of Titanium dioxide (TiO_2) was carried out using $TiOSO_4$ (>29% Ti (as TiO2 basis), Aldrich), ammonia solution (28.0%, Aldrich), benzoic acid, cinnamic acid, salicylic acid and deionized water. In the experiment, 10 g of $TiOSO_4$ was dissolved in 150 ml of deionized water at room temperature. The certain amount of carboxylic acid (1:0.5, 1:1 and 1:2) was dissolved in acetonitrile, and then added into the $TiOSO_4$ solution. The solution was then heated to 80.0 ± 2.0 ºC for 1 h under constant stirring. After that ammonia solution was added dropwise until the solution pH was 7. The solution was left under stirring for a further 1 h. The schematic of the modification of TiO_2 with carboxylic acid is shown in Figure 2.2. The obtained precipitate was washed several times with deionized water and then dried at 60 ºC for 24 h. The powder was calcined in air at 600 ºC for 3 h.

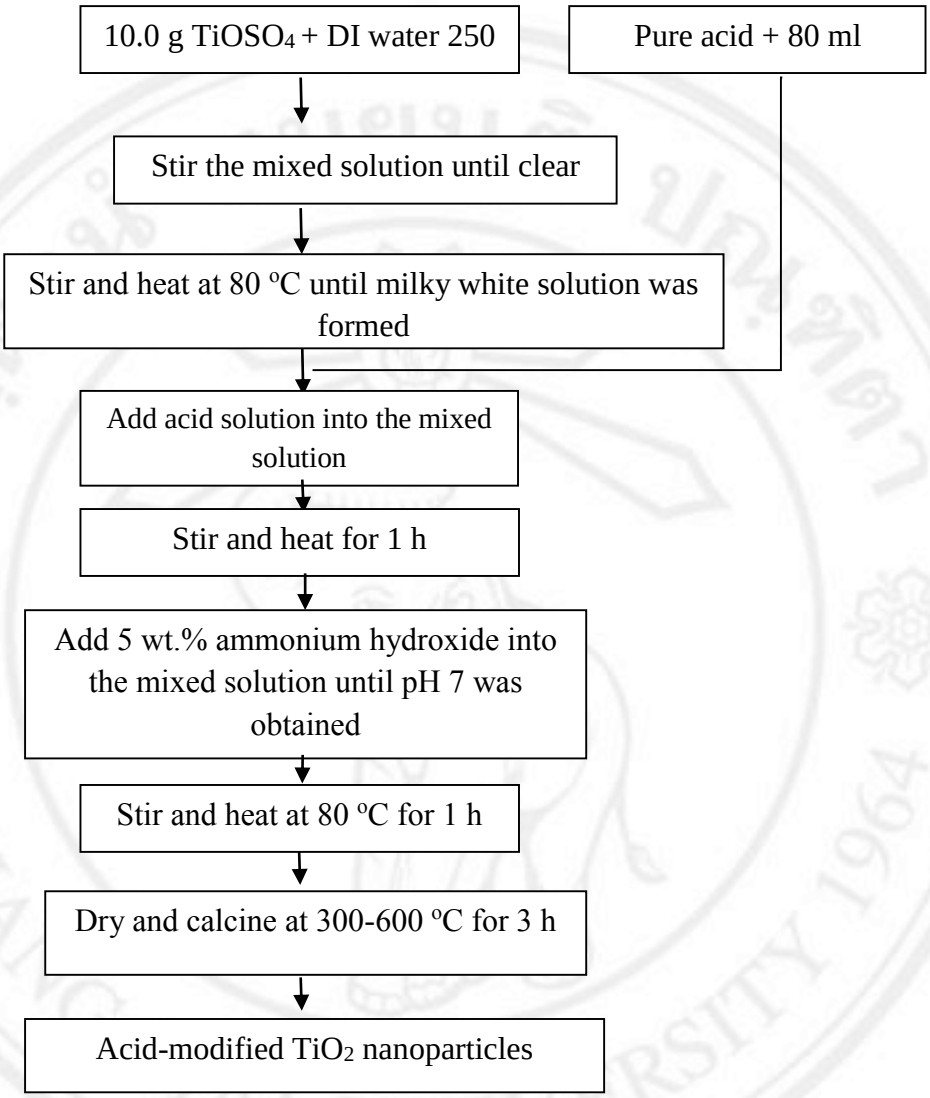

Figure 2.2 The diagram of the modification of TiO_2 using carboxylic acids

2.4 Sample characterization

The characterization of the TiO_2 and TiO_2 modified with carboxylic acid were included X-ray diffraction spectroscopy (XRD), Scanning electron microscopy (SEM), Transmission electron microscopy (TEM), UV-Vis diffuse reflectance spectroscopy (UV-Vis DRS), BET-Specific surface area (SSA), Fourier transform infrared spectrophotometry (FT-IR) and zetasizer nano instrument.

2.4.1 UV-Vis diffuse reflectance spectroscopy (UV-vis DRS) [1], [2]

UV-visible diffuse reflectance has been used widely in band gap approximation and surface characterization. UV-visible diffuse reflectance is an essential tool to investigate a band gap energy. In general electromagnetic radiation can be reflected either in specular mode where the angle of reflectance is equal to the angle of incidence, or diffuse mode where light is scattered in all directions.

UV–vis diffuse reflectance spectra (DRS) data were obtained from the dry-pressed sample disks of TiO_2 nanoparticle by using a scan UV–vis spectroscopy (Lambda 650S) equipped with an integrating sphere assembly, using MgO as reflectance sample. The Kubelka-Munk absorption spectra were calculated by analyzing the reflectance measurement with Kubelka-Munk emission function. The spectra were recorded at room temperature in the range of 200-700 nm. Optical properties of TiO_2 powders were investigated by UV–vis diffuse reflectance spectro photometer (UV–vis DRS, Lambda 650S) equipped with a Harrick Praying Mantis™ diffuse reflectance chamber.

2.4.2 X-ray diffraction (XRD) [1]

XRD technique is an important method to identify non molecular and crystalline substances. It can be used to determine the crystal structure, unit cell parameters, phase content and crystallite size. X-rays are electromagnetic radiation of wavelength around 1 angstrom. Diffraction arises from an interference between in phase adjacent scattering beams (Figure 2.3). When X-rays are scattered by two adjacent parallel planes of atoms or ions in the crystal separated by perpendicular distance or d-spacing, d, the angle of incident at which constructive interference

occurs between beams of wavelength λ, can be related by Bragg's law (equation 2.1).

$$n\lambda = 2d \sin\theta \quad (2.1)$$

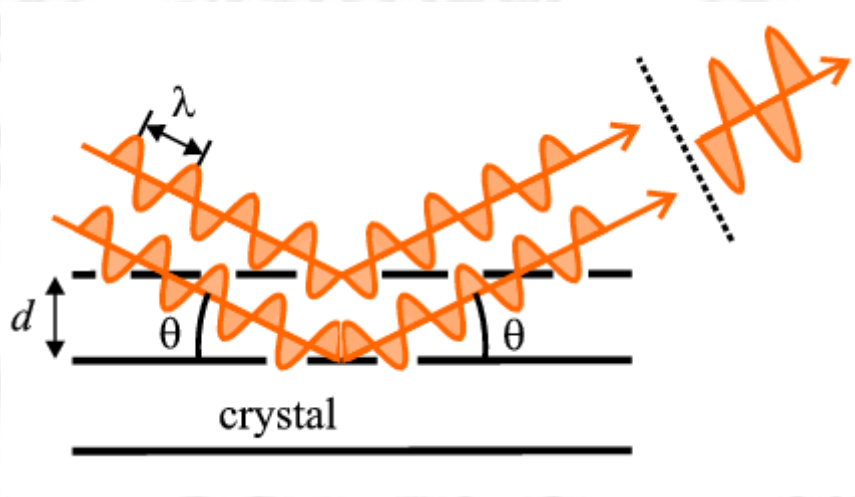

Figure 2.3 Derivation of Bragg's law [3]

There are 2 types of XRD: powder X-ray diffraction and single crystal X-ray diffraction. Powder X-ray diffraction is used to identify polycrystalline materials, which comprises of thousands of crystallites. Whereas single crystal X-ray diffraction is used for single crystal structure determination. Since TiO_2 synthesized in this work is in a polycrystalline form, phase identification is carried out by powder X-ray diffraction. Phase composition of the samples was calculated by using the following equation 2.2 [4]

$$\text{Rutile phase (\%)} = 100/[1+0.89(I_A/I_R)] \quad (2.2)$$

where k is a constant equal to 0.89, and I_A and I_R are the intensities of the anatase (101) and rutile (110) diffraction peaks, respectively.

Apart from phase identification, it can be used to determine approximate crystallite size. The average crystallite size can be estimated from peak broadening by

the Debye-Scherrer equation on the anatase (101) and rutile (110) diffraction peaks [4].

$$D = \frac{k\lambda}{\beta cos\theta} \quad (2.3)$$

where D is the average crystallite size in angstroms, λ is the wavelength of the X-ray radiation (Cu Kα) 0.154056 nm), β is the full width at half-maximum of the highest intensity peak and θ is the radian diffraction angle. k is a dimensionless constant which is taken as 0.89 here, assuming every point on the lattice emits a spherical wave in a two dimensional lattice. k may range from 0.89 to 1.39 depending on the specific geometry of the scattering objects. k = 0.94 for a cubic three dimensional crystal and k = 1.33 for perfectly spherical object.[5]

The crystal structure, phasetransformation and average crystallite size of the TiO_2 nanoparticles were studied by XRD (Rigaku MiniFlex II) with CuKα radiation (1.54Å) over the 2θ range of 20–80º.

2.4.3 EM studies

In order to examine the morphology and topography of very small specimens, electron microscopy will give much more information than optical microscopy. Electron microscopy is a powerful tool to study microstructure of nanomaterials. An electron microscope consists of an electron gun, anode, lens, apertures and image recording. The electron, which is commonly produced by heating a tungsten filament, will be attracted by anode and accelerated down the vacuum column and interact with specimens. The electron microscope uses electrostatic and electromagnetic lenses to control the electron beam and focus it to form an image. Wavelength of the beam might need to be adjusted to close to size of specimens in order to provide more

reaction and get more image resolution. As the electron leaves the filament with high potential energy and reaches the anode with high kinetic energy, conservation of energy is applied as following equation [6]

$eV = 1/2mv^2 = \frac{h^2}{2m\lambda^2}$ (De Broglie equation $p = mv = \frac{h}{v}$)

$$\lambda = \frac{h}{\sqrt{2meV}} \quad (2.4)$$

When *V* is very large, relativistic correction is required because velocity, v, is close to speed of light, *c*.

$$\lambda = \frac{h}{\sqrt{2m_0eV_0(1+\frac{eV_0}{2m_0c^2})}} \quad (2.5)$$

Where $m_0$denotes electron rest mass, V_0 denotes accelerating voltage.

2.4.3.1 Scanning electron microscopy (SEM)

Scanning electron microscope can provide information on surface morphology of the specimen. When the electron beam produced from filament, it can be focused by condenser lens to a spot less than 4 nm and a rectangular raster is scanned over the specimen after passing through two sets of scan coils (Figure 2.4). There are several phenomena occur during primary electron bombarding specimen such as emission of secondary electrons, backscattered electrons, X-rays, photon(light) and absorption of electron by the specimen. The secondary electron detector is generally used for image formation with the scanning electron microscope [7]. The morphology of TiO_2 was examined by SEM, model JEOL JSM6335F.

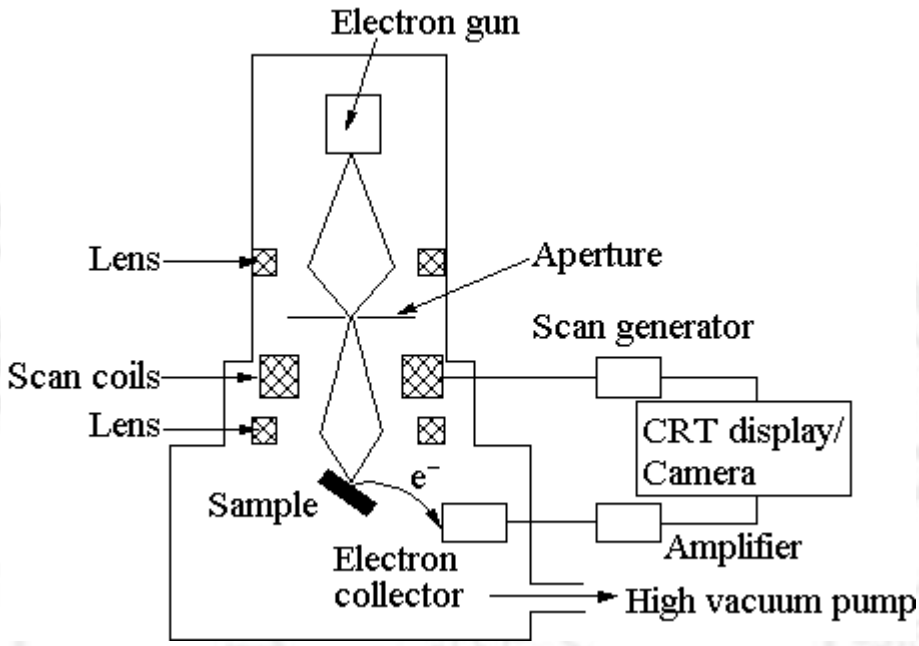

Figure 2.4 An illustration of SEM spectroscope [8]

2.4.3.2 Transmission electron microscope (TEM)

Transmission electron microscope (TEM), electrons are transmitted through the sample. Normally the incident and scattered electrons are referred to as electron beams. In TEM, the electron beam is transmitted through the instrument's optics. The TEM has an electron gun and electromagnetic lenses which include condenser and objective lenses. The condenser lenses converge and control the electron beam and illuminate the sample, and the objective lenses forms the image of the sample and diffraction. The images and diffractions are then magnified by other lenses in the system. A base reference line passing through the centre of all the lenses is called the optic axis of the electron microscope.[9] Transmission electron microscope (Figure 2.5) is used to study thin specimen as the image is formed when

electrons strike the specimen. Phase contrast and diffraction contrast are important factors in image formation of crystalline specimen.[9]

The particle size and microstructural morphology of the nanocrystalline powders were investigated on TEM (JEM-2010).

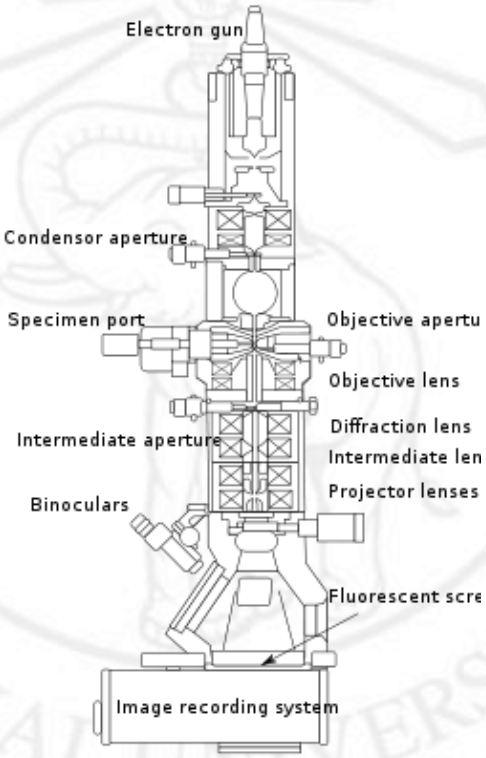

Figure 2.5 An illustation of TEM microscope [10]

2.4.4 Fourier transform infrared spectrophotometry (FT-IR) studies

The region of infrared radiation ordinarily extends from about 2.5 to 16 microns (1 micron = 1 micrometer = 10^{-6} meter). Infrared spectroscopy involves examination of the stretching vibrations. Stretching vibrations change distances between adjacent atoms. Bending vibrations (including scissoring, rocking, twisting, wagging) change bond angles. FT-IR is most useful for identifying chemicals that are

either organic or inorganic. It can be utilized to quantify some components of an unknown mixture. It can be applied to the analysis of solids, liquids, and gasses. The term Fourier Transform Infrared Spectroscopy (FT-IR) refers to a fairly recent development in the manner in which the data is collected and converted from an interference pattern to a spectrum. FT-IR instruments are computerized which makes them faster and more sensitive than the older dispersive instruments.[11]

Fourier transform infrared spectroscopy (FTIR) spectra were recorded in the range of 4000-400 cm^{-1} using a Fourier transform infrared spectrophotometer (FT-IR), 510 Nicolet using compressed KBr disc technique.

2.4.5 BET-Specific surface area (SSA)

The BET method is widely used for the determination of surface areas of solids by physical adsorption of gas molecules, assuming there is no interaction between each layer. Prior to determining the surface area, the adsorbed impurities on the sample surface need to be removed by heating, evacuating and/or flowing gas. Then, the sample is cooled down, usually, with liquid nitrogen. After degassing, an adsorptive gas will be introduced into the chamber and the surface area can be analysed by measuring the volume of gas adsorbed at specific pressures. The BET equation is expressed by [6] :

$$\frac{P}{x(P_0-P)} = \frac{1}{X_m C} + \frac{C-1}{X_m C}\frac{P}{P_0} \qquad (2.6)$$

Where P and P_0 are the equilibrium and the saturation pressure of adsorptive gas at the temperature of adsorption, X is the adsorbed gas quantity and X_m is the monolayer adsorbed gas quantity and C is the BET constant. Equation 2.6 can be plotted as a straight line and X_m is calculated from the slope and intercept. [12]

The surface area (*S*) is then evaluated by equation 2.7 :

$$S = \frac{X_m N_0 A_0}{wM} \quad (2.7)$$

Where N_o is Avogadro's number, A_o is adsorption cross section, *M* is molar volume of adsorptive gas, *w* is mass of adsorbent material. [6]

The Brunauer–Emmett–Teller (BET) specific surface areas (SSA) of pure TiO_2 and TiO_2 modified with carboxylic acid were determined through nitrogen adsorption at 77 K (Micromeritics Tristar 3000). All samples were degassed at 150 °C for 1h before the measurement.

2.4.6 zetasizer nano instrument

The Zetasizer Nano series calculates the zeta potential by determining the Electrophoretic Mobility and then applying the Henry equation. The electrophoretic mobility is obtained by performing an electrophoresis experiment on the sample and measuring the velocity of the particles using Laser Doppler Velocimetry (LDV). The development of a nett charge at the particle surface affects the distribution of ions in the surrounding interfacial region, resulting in an increased concentration of counter ions (ions of opposite charge to that of the particle) close to the surface. Thus an electrical double layer exists around each particle. The liquid layer surrounding the particle exists as two parts; an inner region, called the Stern layer, where the ions are strongly bound and an outer, diffuse, region where they are less firmly attached. Within the diffuse layer there is a notional boundary inside which the ions and particles form a stable entity. When a particle moves (e.g. due to gravity), ions within the boundary move with it, but any ions beyond the boundary do nottravel with the particle. This boundary is called the surface of hydrodynamic shear orslipping plane.

The potential that exists at this boundary is known as the Zeta potential. The magnitude of the zeta potential gives an indication of the potential stability of the colloidal system. A colloidal system is when one of the three states of matter: gas, liquid and solid, are finely dispersed in one of the others. For this technique we are interested in the two states of: a solid dispersed in a liquid, and a liquid dispersed in a liquid, i.e. an emulsion.

The most important factor that affects zeta potential is pH. A zeta potential value on its own without a quoted pH is a virtually meaningless number. Imagine a particle in suspension with a negative zeta potential. If more alkali is added to this suspension then the particles will tend to acquire a more negative charge. If acid is then added to this suspension a point will be reached where the negative charge is neutralised. Any further addition of acid can cause a build up of positive charge. Therefore a zeta potential versus pH curve will be positive at low pH and lower or negative at high pH. The point where the plot passes through zero zeta potential is called the Isoelectric point and is very important from a practical consideration. It is normally the point where the colloidal system is least stable [13]. A typical plot of zeta potential versus pH is shown Figure 2.6.

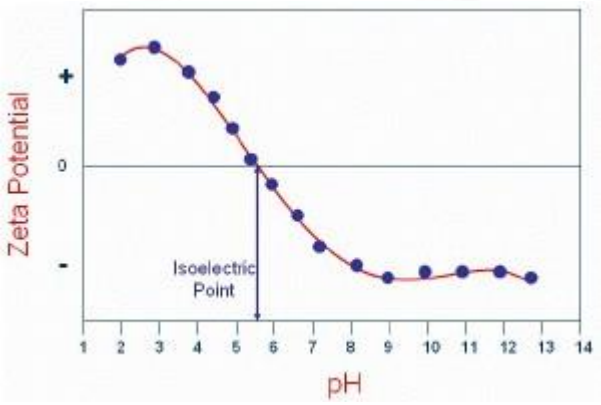

Figure 2.6 A typical plot of zeta potential versus pH [14]

Isoelectric point of the obtained samples was also examined by zetasizer nano instrument (ZS Malvern). The suspension pH were adjusted to 2, 4, 6, 7, 8 and 10 using 0.1 M Sodium hydroxide (NaOH) and 0.1 M Perchloric acid ($HClO_4$).

2.5 Photocatalytic activity studies

A schematic diagram of the spiral photoreactor at CMU [15] was given in Figure 2.7. The spiral photoreactor consisted of (i) 70 cm long spiral reactor. The spiral reactor was made out of borosilicate glass tube with an outside diameter of 5 mm and the wall thickness of 1 mm. Photocatalytic reaction was initiated by illuminating the catalyst suspension in the spiral reactor with UVA lamp (Sylvania blacklight blue, 18W) (ii) The glass spiral filtered with the lamp was covered with aluminum foil to prevent both the intrusions of ambient light and the emission of the harmful UV from the lamp. The attachment to the photoreactor were (iii) a peristaltic pump (iv) a conductivity meter and EUTECH PC 5500 and (v) a gas-liquid separator. All components were connected together using masterflex flexible tubing which was resistant to leaching of any organics.

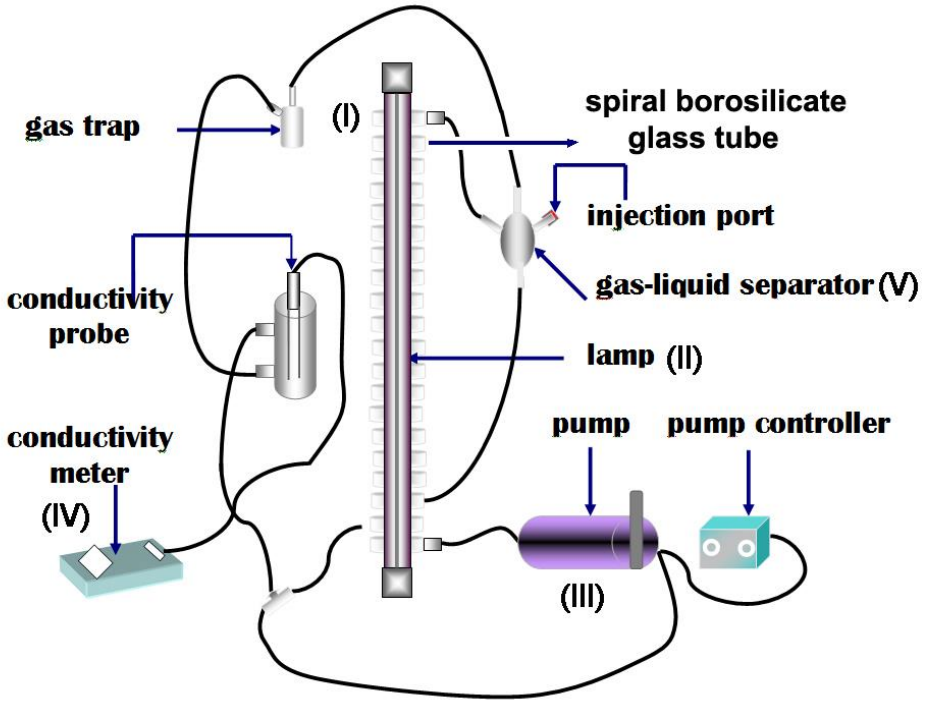

Figure 2.7 Schematic illustration of spiral photoreactor [15]

Photocatalytic activity of the TiO_2 powders was studied on a slurry-type spiral photoreactor centered with a UVA lamp (Sylvania blacklight blue, 18W). The reactor was connected to a conductometer (Eutech PC 5500) for monitoring CO_2 generated as a product of organic compound mineralization. The catalyst suspension (1 g/L) was prepared in deionized water and the suspension pH was adjusted to 7 using 0.1 M NaOH. Prior to catalytic testing, an impurity carbon burn off step was performed by illuminating the catalyst suspension with UVA lamp until the conductivity measurement was constant. A 100 μL of phenol solution, containing 500 μg carbon, was injected into the suspension and dark adsorption of the organic onto the TiO_2 was allowed for 1 h. Photocatalytic mineralization of phenol was initiated by turning on

the UVA lamp and the reaction kinetics were evaluated via the change of conductivity value.

REFERENCES

1. Schiavello, M., *Heterogeneous photocatalysis*. John Wiley & Sons: 1997; Vol. 3.
2. Sirita, J.; Phanichphant, S.; Meunier, F. C., Quantitative analysis of adsorbate concentrations by diffuse reflectance FT-IR. *Analytical chemistry* **2007,** *79* (10), 3912-3918.
3. http://pd.chem.ucl.ac.uk/pdnn/powintro/braggs.htm. (25 June 2013).
4. Behnajady, M.; Eskandarloo, H.; Modirshahla, N.; Shokri, M., Investigation of the effect of sol–gel synthesis variables on structural and photocatalytic properties of TiO_2 nanoparticles. *Desalination* **2011,** *278* (1), 10-17.
5. Spurr, R. A.; Myers, H., Quantitative analysis of anatase-rutile mixtures with an X-ray diffractometer. *Analytical Chemistry* **1957,** *29* (5), 760-762.
6. German, R. M., *Powder metallurgy science*. Metal Powder Industries Federation Princeton, NJ: 1984.
7. http://www.purdue.edu/REM/rs/sem.htm. (25 June 2013).
8. http://www.chm.bris.ac.uk/pt/diamond/stuthesis/chapter2.htm. (25 June 2013).
9. Gai, P. L.; Boyes, E. D., *Electron microscopy in heterogeneous catalysis*. CRC Press: 2010.
10. http://commons.wikimedia.org/wiki/File:Scheme_TEM.gif. (25 June 2013).
11. Dilling, W. L.; Dilling, M. L., Organic Chemistry. *Van Nostrand's Encyclopedia of Chemistry*.

12. P. Atkins, T. O., J. Rourke, M. Weller and F. Armstrong, Shriver &; Atkins Inorganic Chemistry, O. U. p., 4th edn. Ch.6, pp. 169-; 195.

13. http://www.nbtc.cornell.edu/facilities/downloads/Zetasizer%20chapter%2016.pdf. (25 June 2013)

14. http://www.azom.com/article.aspx?ArticleID=3939. (25 June 2013)

15. Wetchakun, N., Effect of transition metal ion doping on the photocatalytic activity of titanium dioxide. *The Graduate School Chiang Mai University* **2008,** (73-82).